Epitaxial growth and transport properties of compressively-strained Ba_2IrO_4 films

Y.Q. Zhao[1], H. Zhang[1], X.B. Cai[2], W. Guo[1], D.X. Ji[1], T.T. Zhang[1], Z.B. Gu[1], J. Zhou[1], Y. Zhu[3,*] and Y.F. Nie[1,†]

[1] *National Laboratory of Solid State Microstructures, College of Engineering and Applied Sciences, and Collaborative Innovation Center of Advanced Microstructures, Nanjing University, Nanjing 210093, China*

[2] *Department of Physics, The Hong Kong University of Science and Technology, Clear Water Bay, Kowloon, Hong Kong, China*

[3] *Department of Applied Physics, Research Institute for Smart Energy, The Hong Kong Polytechnic University, Hung Hom, Kowloon, Hong Kong, China.*

[*] Email: yezhu@polyu.edu.hk

[†] Email: ynie@nju.edu.cn

Ba_2IrO_4 is a sister compound of the widely investigated Sr_2IrO_4 but with no octahedral rotations and canted magnetic moments, providing a great candidate to search for novel high T_c superconductivity. In this work, we synthesize Ba_2IrO_4 epitaxial films by reactive molecular beam epitaxy and explore their crystalline structure and transport properties under biaxial strain. High resolution scanning transmission electron microscopy and X-ray diffraction confirm the high quality of the crystalline structure with partial strain relaxation. With the residual compressive epitaxial strain, Ba_2IrO_4 exhibits a strain-driven enhancement of the conductivity, consistent with the bandgap narrowing in the first-principles theoretical calculations.

I. INTRODUCTION

The strong spin-orbit coupling and its interplay with electron correlations in 5*d* transition metal oxides (TMOs) give rise to the intriguing $J_{eff} = 1/2$ antiferromagnetic Mott insulator state in layered iridate Sr_2IrO_4.[1,2] Sr_2IrO_4 share many common features with the high-T_c cuprates, such as layered K_2NiF_4 crystal structure, Fermi arcs,[3,4] antiferromagnetic Mott ground state[5] and V-shape energy gap, etc.[6-9] As such, Sr_2IrO_4 is predicted to be a new type of high-temperature superconductor upon electron-doping.[10,11] But direct experimental evidences, such as zero resistance and Meissner effect, are still lacking.[12-16]

In contrast to the sizable octahedral rotations and net canted magnetic moments in the IrO_2 planes in Sr_2IrO_4, which may suppress superconductivity, its sister compound Ba_2IrO_4 (BIO) exhibits zero or negligible octahedral rotations and canted moments, making it more similar to the parent compound

The following publication Zhao, Y. Q., Zhang, H., Cai, X. B., Guo, W., Ji, D. X., Zhang, T. T., ... & Nie, Y. F. (2021). Epitaxial growth and transport properties of compressively-strained Ba2IrO4 films. Chinese Physics B, 30(8), 0874014.0 is availalble at https://doi.org/10.1088/1674-1056/abea97

of high-T_c cuprates.[17] However, the sample synthesis of Ba_2IrO_4 is challenging by high-pressure[17] due to the metastable properties. The metal-insulator (M-I) transition can be observed under high pressure[18]. The synthesis of Ba_2IrO_4 thin films by the method of pulsed laser deposition (PLD)[19] and molecular beam epitaxy (MBE)[20] was previously reported. Experimental works have demonstrated that epitaxial strains can tune the electronic structure of Sr_2IrO_4,[21] but the strain effects on Ba_2IrO_4 films remains unclear.

In this work, we synthesize Ba_2IrO_4 epitaxial films by reactive MBE and explore its crystalline structure, transport and electronic properties by X-ray diffraction (XRD), scanning transmission electron microscopy (STEM) and first-principles calculations.

II. EXPERIMENTAL SECTION

Epitaxial Ba_2IrO_4 (BIO) films are grown on various single-crystal substrates in ozone-assisted oxide molecular beam epitaxy system (DCA R450). During film growth, the substrates are heated to 800°C (measured by a pyrometer) in a distilled 100% O_3 at a background pressure of 1×10^{-6} Torr.[20] Barium atoms are evaporated using a Knut effusion cell and iridium atoms are evaporated using an electron-beam evaporator since the evaporation temperature of iridium is beyond what a typical Knut effusion cell can reach. The film growth rate is about 0.2~0.3 Å/s and excess Ir flux is supplied to compensate the volatility of IrO_x at the growth temperature.[22] Since bare BIO films are found to degrade quickly in air, we cap BIO films with 10 layers $SrTiO_3$, which can protect and stabilize BIO film in ambient conditions.

To explore the strain effects, three different single-crystal substrates are used, namely, $(LaAlO_3)_{0.3}(Sr_2AlTaO_6)_{0.7}$ (100) (LSAT), $SrTiO_3$ (100) (STO) and $GdScO_3$ (110) (GSO). Bulk BIO has lattice parameters of 4.030 Å in-plane and 13.333 Å out-of-plane.[17] The pseudo-cubic lattice parameters of the substrates and their nominal lattice mismatch with BIO are listed in Table 1. The optimal growth condition of BIO films strongly depends on the substrate. BIO films can be grown directly on STO and GSO substrates but a direct growth of BIO on LSAT only yields poor quality films with impurity phases. By growing a buffer layer of 5-unit cell of $SrTiO_3$, high quality BFO films are obtained on LSAT substrate. Moreover, we get best quality BIO films with the nominal growth Ba/Ir flux ratio of 2:1.13, 2:1.05 and 2:1.33 on LSAT, STO and GSO substrates, respectively.

For all substrates, we deposit an extra BaO layer before opening the shutters to co-deposit both Ba and Ir species simultaneously. A direct deposition of BIO films without the pre-deposition step on substrates exhibits extra diffraction peaks in the RHEED patterns, indicating the formation of impurity phases.

The quality of BIO films is characterized by high-resolution Bruker “D8 Discover” x-ray diffractometer (XRD, Cu Kα radiation, λ=1.5418 Å). Scanning transmission electron microscopy (STEM) is performed by JEOL ARM 200CF with the ASCOR probe corrector to investigate the microstructure of cross-sectional BIO films. High-angle annular dark field (HAADF) imaging was conducted with a 26 mrad convergence semi-angle and a 110 mrad inner collection semi-angle. Temperature-dependent electronic transport properties are measured by a conventional four-probe approach in the Van der Pauw method. The density functional theory (DFT) calculations are also performed to investigate the stain-driven electronic structure evolution.

III. RESULTS AND DISCUSSION

Figure 1(a) shows the crystal structure of BIO. All BIO films in this work are about 15 nm thick. The films are grown on three different substrates and undergo compressive strain from substrates. In figure 1(b), the X-ray 2θ - ω scans of specimens exhibit sharp 00l-peaks, indicating the high crystalline quality of the single-crystal BIO films.

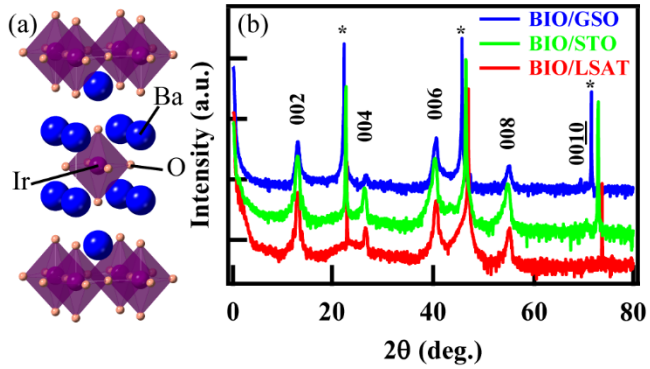

Figure. 1. (a) Tetragonal structure of bulk Ba_2IrO_4. (b) XRD $2\theta - \omega$ scans of the BIO films grown on the LSAT (red), STO (green) and GSO (blue) substrates. The asterisks (*) correspond to the peaks from substrates.

To explore the in-plane lattice constants and strain state of the films, we perform reciprocal space mapping (RSM) on the films. Figure 2 presents the RSM for all BIO films around the $(103)_p$ reflections of substrates. The results show that the H values of all BIO films deviate from the substrate reflections, indicating the partial relaxation of the in-plane strain due to the large lattice mismatches. The detail lattice mismatch, in-plane (a) and out-of-plane (c) lattice parameters determined by RSM are listed in Table I. The real strain values depend on the combination of lattice mismatch and strain relaxation. The extracted in-plane compressive strain ($\varepsilon_{xx} = (a_{film} - a_{bulk})/a_{bulk} \times 100\%$) are -0.74%, -1.24% and -0.99% for BIO films grown on GSO, STO and LSAT substrates, respectively. The absolute strain increases with the mismatch for BIO films grown on GSO and STO and then start to decrease again in BIO film grown on LSAT since the lattice mismatch (-4.13%) is so large and the relaxation effect is prominent in BIO/LSAT.

Table 1. Lattice parameters, lattice mismatches and corresponding epitaxial strains of BIO films.

Substrate	In-plane a_{sub}(Å)	Lattice mismatch (%)	a_{BIO}(Å)	c_{BIO}(Å)	ε_{xx}(%)
GSO (110)	3.96	-1.77	4.00	13.30	-0.74
STO (100)	3.90	-3.33	3.98	13.40	-1.24
LSAT (100)	3.87	-4.13	3.99	13.34	-0.99

1. In here, a_{sub} of GSO is a pseudo-cubic lattice constant.
2. lattice mismatch (%) $= (a_{sub} - a_{bulk})/\ a_{sub} \times 100\%$.
3. $\varepsilon_{xx} = (a_{film} - a_{bulk})/\ a_{bulk} \times 100\%$.

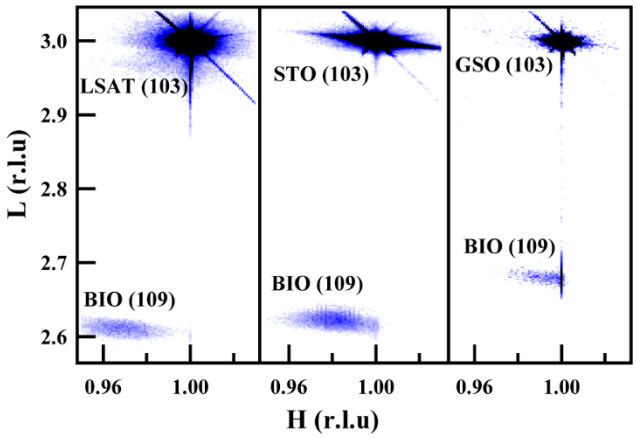

Figure. 2. Reciprocal space maps (RSM) of BIO (109) reflections near the pseudo-cubic (103) peak of LSAT, STO and GSO substrates.

High-resolution STEM annular dark field (ADF) imaging on the cross-section membranes of BIO/substrate interfaces along the [010] zone axis is shown in Figure 3. STEM-ADF images show the high-quality stacking of BaO and IrO_2 layers, which is consistent with the atomic model in Figure 1(a). The lattice relaxation of BIO film on the STO/LSAT substrate is visible in Figure 3(a) as the slight BIO/STO interface degradation.

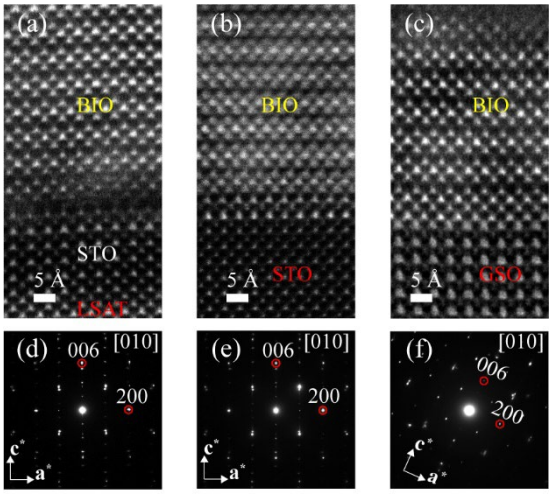

Figure. 3. (a), (b) and (c) are cross-sectional STEM-ADF images projected along the [010] direction near the BIO/substrate interfaces. (d), (e) and (f) are selected-area electron diffraction patterns of the observed areas.

Figure 4 shows the sheet resistivities of BIO films as the function of temperature on three substrates. All samples show a typical insulating behavior with negative $d\rho/dT$. The increasing compressive strains supplied by substrates can reduce the resistivity of BIO films. The 3D Mott variable-range hopping (3D Mott-VRH) model is adopted here to fit the data from room temperature to 100 K, and the fitting formula is $\rho(T) = \rho_0 e^{(T_M/T)^{1/4}}$, where ρ_0 is the resistivity coefficient, and T_M is the characteristic temperature.[23-25] The fitting results of $ln\rho$ versus $T^{-1/4}$ are presented in the inset. According to the criterion of 3D Mott-VRH, the ratio of average hopping distance R_M and localization length a must be larger than 1. It means that $\frac{R_M}{a} = \frac{3}{8}\left(\frac{T_M}{T}\right)^{1/4} > 1$ should be satisfied. By our fitting and calculating, as shown in the inset, the ratio of R_M/a is larger than 5 for all samples.

We consider that the 3D Mott-VRH is dominant in our BIO transport mechanisms.

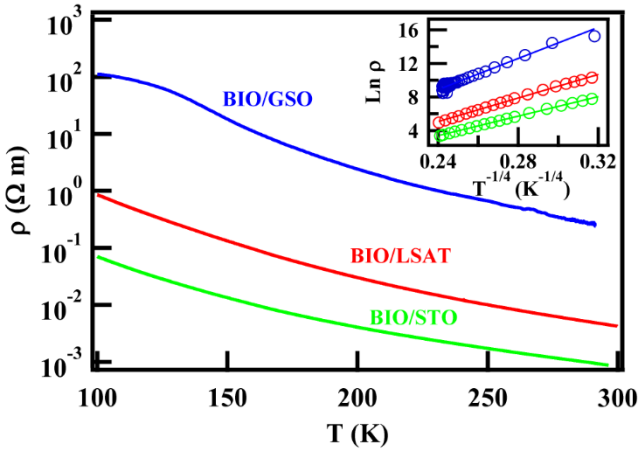

Figure. 4. Temperature-dependent resistivities of BIO films. Logarithmic resistivities versus $T^{-1/4}$ (little circles) and fitted lines according to the 3D Mott-VRH model (straight lines) are shown in the inset.

The electron density of states (DOS) of BIO are calculated by the first-principles density functional theory (DFT) with a generalized gradient approximation implemented in the Vienna ab initio simulation package (VASP) code,[26,27] in which the projected augmented wave method[28,29] and the Perdew-Burke-Ernzerhof exchange-correlation functional[30] are used. The plane-wave cutoff energy was 520 eV throughout the calculations. The smallest spacing between the k-points is 0.2 $Å^{-1}$ (KSPACING=0.2). A $\sqrt{2} \times \sqrt{2} \times 1$ supercell is used to accommodate the anti-ferromagnetic structure in Ba_2IrO_4. The electron correlation of the Ir ions is considered by the DFT+U scheme with the effective Hubbard U=2.0 eV. Due to the heavy Ir ions, the spin-orbital coupling (SOC) effect is also added in our calculations.

The lattice constants and atomic positions are both relaxed to simulate the unstrained bulk BIO and the final optimized lattice constants are a = 4.001 and c = 13.283 Å, which are well consistent with the experimental results. Then the in-plane compressing effect is simulated by reducing the lattice constant (a) with a fixed ratio of 1%, 2%, and 4% while the out-of-plane lattice constant (c) and atomic positions are free to be relaxed. As shown in Figure 5, the total DOS indicates a clear energy gap near the fermi level (red dash line) for the unstrained condition. The band gap gradually shrinks and disappears at an in-plane strain of -2%. This tendency is in accordance with transport experimental results that the conductivity of BIO films increases with increasing in-plane compressive strains. Projected -DOS on O-2p orbital, iridate t_{2g} and e_g orbital, respectively. By the increasing DOS of Ir-t_{2g} and O-2p near the fermi level with increasing in-plane compressive strains, it seems that in-plan compressive strains enhance the orbital hybridizations O-2p to Ir-t_{2g}, which increase the electronic orbital overlap making the resistance of BIO films decrease from GSO to STO substrate. This DFT simulation can explain enhancing conducting properties of our experimental results well.

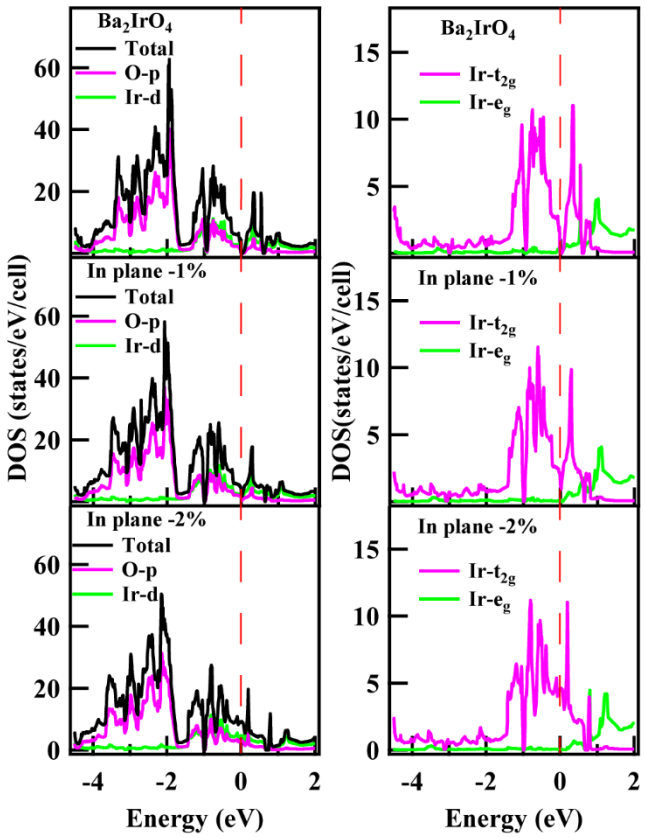

Figure. 5. The total and projected densities of states (DOS) of BIO, showing a gap narrowing and increase of DOS under in-plane compressive strain. The dash lines mark the Fermi energy.

IV. CONCLUSIONS

In summary, we successfully grow Ba_2IrO_4 films on LSAT, STO and GSO substrates by reactive molecular beam epitaxy. XRD and STEM measurements confirm that all films have high crystalline quality. Three different strain states have been achieved on these substrates with partial strain relaxation due to the relatively large lattice mismatch. The transport measurements show an enhancement of the conductivity under increasing in-plane compressive strains. DFT calculations also show a band gap closing and an increase of DOS near the Fermi level under compressive strain due to the overlap of Ir-t_{2g} and O-2*p* orbitals.

ACKNOWLEDGMENTS

This study is supported by the National Natural Science Foundation of China (NSFC Grant Nos. 11774153, 11861161004, 51672125, and 51772143), the Fundamental Research Funds for the Central Universities (Grant No. 0213-14380167), and the Hong Kong Research Grants Council (RGC) through the NSFC-RGC Joint Research Scheme (Grant No. N_PolyU531/18).

References:

[1]B. J. Kim, H. Jin, S. J. Moon, J. Y. Kim, B. G. Park, C. S. Leem, J. Yu, T. W. Noh, C. Kim, S. J. Oh, J. H. Park, V. Durairaj, G. Cao, and E. Rotenberg, Phys. Rev. Lett. **101,** 076402 (2008).

[2]B. J. Kim, H. Ohsumi, T. Komesu, S. Sakai, T. Morita, H. Takagi, and T. Arima, Science **323,** 1329 (2009).

[3]Y. K. Kim, O. Krupin, J. D. Denlinger, A. Bostwick, E. Rotenberg, Q. Zhao, J. F. Mitchell, J. W. Allen, and B. J. Kim, Science **345,** 187 (2014).

[4]A. de la Torre, S. McKeown Walker, F. Y. Bruno, S. Riccó, Z. Wang, I. Gutierrez Lezama, G. Scheerer, G. Giriat, D. Jaccard, C. Berthod, T. K. Kim, M. Hoesch, E. C. Hunter, R. S. Perry, A. Tamai, and F. Baumberger, Phys. Rev. Lett. **115,** 176402 (2015).

[5]J. Kim, D. Casa, M. H. Upton, T. Gog, Y.-J. Kim, J. F. Mitchell, M. van Veenendaal, M. Daghofer, J. van den Brink, G. Khaliullin, and B. J. Kim, Phys. Rev. Lett. **108,** 177003 (2012).

[6]Y. K. Kim, N. H. Sung, J. D. Denlinger, and B. J. Kim, Nat. Phys. **12,** 37 (2016).

[7]Y. J. Yan, M. Q. Ren, H. C. Xu, B. P. Xie, R. Tao, H. Y. Choi, N. Lee, Y. J. Choi, T. Zhang, and D. L. Feng, Physical Review X **5,** 041018 (2015).

[8]L. Zhao, D. H. Torchinsky, H. Chu, V. Ivanov, R. Lifshitz, R. Flint, T. Qi, G. Cao, and D. Hsieh, Nat. Phys. **12,** 32 (2016).

[9]I. Battisti, K. M. Bastiaans, V. Fedoseev, A. de la Torre, N. Iliopoulos, A. Tamai, E. C. Hunter, R. S. Perry, J. Zaanen, F. Baumberger, and M. P. Allan, Nat. Phys. **13,** 21 (2017).

[10]F. Wang and T. Senthil, Phys. Rev. Lett. **106,** 136402 (2011).

[11]H. Watanabe, T. Shirakawa, and S. Yunoki, Phys. Rev. Lett. **110,** 027002 (2013).

[12]C. Cosio-Castaneda, G. Tavizon, A. Baeza, P. de la Mora, and R. Escudero, J. Phys.: Condens. Matter **19,** 446210 (2007).

[13]O. B. Korneta, T. Qi, S. Chikara, S. Parkin, L. E. De Long, P. Schlottmann, and G. Cao, Physical Review B **82,** 115117 (2010).

[14]D. Haskel, G. Fabbris, M. Zhernenkov, P. P. Kong, C. Q. Jin, G. Cao, and M. van Veenendaal, Phys. Rev. Lett. **109,** 027204 (2012).

[15]M. Souri, J. G. Connell, J. Nichols, J. Terzic, G. Cao, and A. Seo, J. Appl. Phys. **126,** 185101 (2019).

[16]W. Guo, D. X. Ji, Z. B. Gu, J. Zhou, Y. F. Nie, and X. Q. Pan, Physical Review B **101,** 085101 (2020).

[17]H. Okabe, M. Isobe, E. Takayama-Muromachi, A. Koda, S. Takeshita, M. Hiraishi, M. Miyazaki, R. Kadono, Y. Miyake, and J. Akimitsu, Physical Review B **83,** 155118 (2011).

[18]H. Okabe, N. Takeshita, M. Isobe, E. Takayama-Muromachi, T. Muranaka, and J. Akimitsu, Physical Review B **84,** 115127 (2011).

[19]J. Nichols, O. B. Korneta, J. Terzic, G. Cao, J. W. Brill, and S. S. A. Seo, Appl. Phys. Lett. **104,** 121913 (2014).

[20]M. Uchida, Y. F. Nie, P. D. C. King, C. H. Kim, C. J. Fennie, D. G. Schlom, and K. M. Shen, Physical Review B **90,** 075142 (2014).

[21]J. Nichols, J. Terzic, E. G. Bittle, O. B. Korneta, L. E. De Long, J. W. Brill, G. Cao, and S. S. A. Seo, Appl. Phys. Lett. **102,** 141908 (2013).

[22]E. H. P. Cordfunke and G. Meyer, Recueil des Travaux Chimiques des Pays-Bas **81,** 495 (1962).

[23]M. Ge, T. F. Qi, O. B. Korneta, D. E. De Long, P. Schlottmann, W. P. Crummett, and G. Cao, Physical Review B **84,** 100402 (2011).

[24]N. F. Mott, J. Non-Cryst. Solids **1,** 1 (1968).

[25]R. Rosenbaum, Physical Review B **44,** 3599 (1991).

[26]G. Kresse and J. Furthmüller, Computational Materials Science **6,** 15 (1996).

[27]G. Kresse and J. Furthmüller, Physical Review B **54,** 11169 (1996).

[28]P. E. Blöchl, Physical Review B **50,** 17953 (1994).

[29]G. Kresse and D. Joubert, Physical Review B **59,** 1758 (1999).

[30]J. P. Perdew, A. Ruzsinszky, G. I. Csonka, O. A. Vydrov, G. E. Scuseria, L. A. Constantin, X. Zhou, and K. Burke, Phys. Rev. Lett. **100,** 136406 (2008).